SMOS-derived Antarctic thin sea-ice thickness: data description and validation in the Weddell Sea

Lars Kaleschke[1,*], Xiangshan Tian-Kunze[1,*], Stefan Hendricks[1], and Robert Ricker[2]

[1]Alfred Wegener Institute, Helmholtz Centre for Polar and Marine Research, Bremerhaven, Germany
[2]NORCE Norwegian Research Center, Tromsø, Norway
[*]These authors contributed equally to this work.

Correspondence: Lars Kaleschke (lars.kaleschke@awi.de)

Abstract. Accurate satellite measurements of the thickness of Antarctic sea ice are urgently needed but pose a particular challenge. The Antarctic data presented here were produced using a method to derive the sea-ice thickness from 1.4 GHz brightness temperatures previously developed for the Arctic, with only modified auxiliary data. The ability to observe thin sea-ice thicknesses using this method is limited to cold conditions, meaning it is only reasonable during the freezing period, typically March to October. The SMOS level 3 sea-ice thickness product contains estimates of the sea-ice thickness and its uncertainty up to a thickness of about 1 m. The sea-ice thickness is provided as daily average on a polar stereographic projection grid with a sample resolution of 12.5 km, while the SMOS brightness temperature data used has a footprint size of about 35-40 km in diameter. Data from SMOS have been available since 2010, and the mission's operation has been extended to continue until at least the end of 2025.

Here we compare two versions of the SMOS Antarctic sea-ice thickness product which are based on different level 1 input data (v3.2 based on SMOS L1C v620, and v3.3 based on SMOS L1C 724). A validation is performed to generate a first baseline reference for future improvements of the retrieval algorithm and synergies with other sensors.

Sea-ice thickness measurements to validate the SMOS product are particularly rare in Antarctica, especially during the winter season and for the valid range of thicknesses. From the available validation measurements, we selected datasets from the Weddell Sea that have varying degrees of representativeness: Helicopter-based EM Bird (HEM), Surface and Under-Ice Trawl (SUIT), and stationary Upward-Looking Sonars (ULS). While the helicopter can measure hundreds of kilometers, the SUIT's use is limited to distances of a few kilometers and thus only captures a small fraction of an SMOS footprint. Compared to SMOS, the ULS are point measurements and multi-year time series are necessary to enable a statistically representative comparison. Only four of the ULS moorings have a temporal overlap with SMOS in the year 2010.

Based on selected averaged HEM flights and monthly ULS climatologies we find a small mean difference (bias) of less than 10 cm and a root-mean-square deviation of about 20 cm with a correlation coefficient R>0.9 for the valid sea-ice thickness range between zero and about one meter. The SMOS sea-ice thickness showed an underestimate of about 40 cm with respect to the less representative SUIT validation data in the marginal ice zone. Compared with sea-ice thickness outside the valid range we find that SMOS strongly underestimates the real values which underlines the need for combination with other sensors such as altimeters.

In summary, the overall validity of the SMOS sea-ice thickness for thin sea-ice up to a thickness of about 1 m has been demonstrated through validation with multiple datasets. To ensure the quality of the SMOS product, an independent regional sea-ice extent index was used for control. We found that the new version v3.3 is slightly improved in terms of completeness, indicating less missing data. However, it is worth noting that the general characteristics of both datasets are very similar, also

30 with the same limitations. Archived data are available on the PANGAEA repository at https://doi.org/10.1594/PANGAEA. 934732, (Tian-Kunze and Kaleschke, 2021) and operationally via https://spaces.awi.de/display/CS2SMOS.

1 Introduction

Antarctic sea ice has very different characteristics compared with that in the Arctic (Eicken et al., 1995; Wever et al., 2021b). Antarctic sea ice is dominated by first-year ice, with multi-year ice mainly distributed in the western Weddell Sea (Worby et al.,

35 2008). The extent of Antarctic sea ice includes twice as much seasonal sea-ice as in the Arctic, but half as much perennial ice as in the Arctic (Stammerjohn and Maksym, 2017). In contrast to the dramatic sea-ice retreat observed in the Arctic the last two decades (Stroeve et al., 2012; Meier et al., 2014), the sea ice extent in the Antarctic showed little change or even slight increasing trends (Zhang, 2007; Holland et al., 2014; Parkinson and Cavalieri, 2012; Allan et al., 2021). However, the situation has changed recently and record low sea-ice extent anomalies in 2022 and 2023 prompt for further research (Voosen, 2023;

40 Gómez-Valdivia et al., 2023; Li et al., 2023; Zhou et al., 2023).

Although Antarctic sea-ice concentration has been monitored from space since five decades, information about the thickness has been elusive until the launch of dedicated altimeter missions (Giles et al., 2008; Kurtz et al., 2012; Zwally et al., 2008). Sea-ice thickness up to 1 m, further referred to as thin ice, can be also be estimated from brightness temperatures such as measured by the L-band radiometer on board of ESA's Soil Moisture and Ocean Salinity mission SMOS. However a thorough validation

45 has been carried out so far only for the northern hemisphere (Kaleschke et al., 2012; Tian-Kunze et al., 2014; Huntemann et al., 2014; Maaß et al., 2015; Kaleschke et al., 2016). Due to the broad swath-width of about 1000 km, SMOS provides daily coverage and is thus complementary to altimeter sensors which measure only along a narrow profile (Ricker et al., 2017).

The Scientific Committee on Antarctic Research (SCAR) Antarctic Sea Ice Processes and Climate (ASPeCt) program has collected ship-born observations over two decades (between 1981 and 2005) and provided one of the most informative map

50 about the distribution of sea-ice thickness in the Antarctic (Worby et al., 2008). However, due to the harsh conditions in the Antarctic during most time of the year, continuous Antarctic-wide observations are lacking, therefore, it is difficult to assess the seasonal and regional variability based on the sparse estimates from ship observations. Giles et al. (2008) compared the ASPeCt data with seven years ice elevation data from ERS radar altimetry and found general agreement in the climatology, but discrepancies in average sea-ice thickness estimates, which could be caused by snow cover and under sampling of ridges in the

55 ASPeCt data.

The influence of snow on the sea-ice, which is often flooded with seawater, leads to high uncertainty for sea-ice thickness estimates by radar altimeters such as ESA's CryoSat2 (Laxon et al., 2013; Ricker et al., 2014). Sea-ice freeboard derived from laser altimeters on board of NASA's Ice, Cloud, and land Elevation Satellites (ICESat and ICESat-2) suffers from the large

uncertainty in the estimation of snow mass on sea ice (Kern and Spreen, 2015; Kern et al., 2016). Kacimi and Kwok (2020)
60 found that 60-70% of the total freeboard measured by ICESat-2 altimeter consists of snow. Sea-ice thickness and volume in the
Antarctic has been analyzed by (Kurtz et al., 2012) using ICESat laser altimetry data for the period of 2003-2008, assuming
that the snow-ice interface is at sea level. No significant trend has been observed. The results were undermined by the large
uncertainties in thickness and volume calculation. Xu et al. (2021) investigated the consistency of total freeboard between
ICESat and ICESat-2, and used an empirical relation between total freeboard, sea ice thickness, and snow depth to derive a
65 circum-Antarctic sea ice thickness trend over the years 2003 to 2020, with missing data from 2009 to 2018. The CRYO2ICE
campaign with optimized orbital overlaps of CryoSat-2 and ICESat-2 will potentially help to derive the snow depth through the
difference in penetration but difficulties in laser-radar comparisons will also remain due to the sampling discrepancies (Fons
et al., 2021).

There are many different ways to measure the sea-ice thickness with different uncertainties applicable on different spatial
70 and temporal scales. The most accurate measurements are the in situ drill holes which allow not only to determine the sea-ice
and snow thickness but also the freeboard level. This method is a time-consuming procedure and strictly limited to in situ field
campaigns at limited locations, thus not representative for large scale sea-ice thickness distributions.

Airborne validation campaigns like NASA's Operation IceBridge or ESA's recent 2022 CryoVEx/DEFIANT Antarctica
campaign for the CRYO2ICE missions were always carried out during the summer months for logistical reasons. The SMOS
75 sea-ice thickness retrieval method is not applicable in the mild temperatures encountered between November and January
and therefore these airborne campaign data cannot be used for validation. Ice-mass balance buoys are usually deployed on
relatively thick sea ice exceeding the limit of the SMOS retrieval method and are therefore also not directly usable for the
validation (Wever et al., 2021a).

Stationary Upward looking sonars (ULS) or Acoustic Doppler Current Profiler (ADCP) allows to determine the ice draft
80 (bottom below water level) over a long period (Behrendt et al., 2015; Belter et al., 2020). Distance measurements from below
are more accurate than freeboard measurements by laser/radar altimeter because of the similar density of sea ice and water
(Belter et al., 2020). Ice draft measurements can be stationary (moored ULS or ADCP) or along profiles with the Surface and
Under-Ice Trawl (SUIT) which has to be drawn by a vessel like Polarstern.

The electromagnetic induction (EM) method allows to measure the total thickness of sea ice and snow with a good accuracy
85 (Haas et al., 2009). The EM method can be applied on a sled, from a ship, or from an airborne platform (fixed-wing aircraft or
helicopter). Airborne EM data have the advantage to resolve the sub-grid-scale variability of sea-ice thickness within a SMOS
footprint while at the same time providing a reasonable representativity. Airborne EM measurements have been compared
with SMOS sea-ice thickness data in previous studies (Tian-Kunze et al., 2014; Kaleschke et al., 2016). The SMOS sea-ice
thickness estimate includes a statistical correction to account for the thickness distribution function. Therefore, the mean rather
90 than the mode of the EM-measured ice thicknesses is compared against the SMOS sea-ice thickness. The EM-measured sea-ice
thickness is the total thickness, i.e. snow+ice, whereas SMOS sea-ice thickness does not include the snow layer.

In this paper, we present two different versions of the SMOS-derived pan-Antarctic thin sea-ice thickness data from 2010
to 2020 (v3.2) and to 2023 (v3.3). The same retrieval procedure as in the Arctic (Tian-Kunze et al., 2014) was applied here to

Antarctica, but with adjusted auxiliary data fields. The retrieved SMOS sea-ice thickness is compared with in situ measurements
95   from ULS, SUIT and Helicopter-based EM (HEM) in the Atlantic sector of Antarctic, namely the Weddell Sea. The algorithm
version v3.2 is based on SMOS L1C brightness temperature version v620 input data, as a reference for the PANGAEA data
repository at https://doi.org/10.1594/PANGAEA.934732. In addition, we perform quality control using independent passive
microwave data. The quality control includes also the current operational SMOS sea-ice thickness data, version v3.3, based on
SMOS L1C brightness temperature version v724.

100   ## 2   Data

2.1   Data used for the SMOS sea ice retrieval

The basis of SMOS sea ice thickness retrieval is the brightness temperature measured by the SMOS payload Microwave
Imaging Radiometer using Aperture Synthesis (MIRAS) at L-band. Furthermore, SMOS sea-ice thickness retrieval needs two
auxilliary data sets: one is atmospheric reanalysis data; the other is sea surface salinity climatology.

105   ### 2.1.1   Gridded L3B SMOS brightness temperature

MIRAS measures the brightness temperatures in full polarization with incidence angles ranging from 0° to 65° (Kerr et al.,
2001; Mecklenburg et al., 2016). The hexagon-like, two-dimensional snapshots measure one or two of the Stokes components in
the antenna reference frame. Horizontally and vertically polarized brightness temperatures are measured by separate snapshots.
SMOS has a spatial resolution of about 35 km at nadir, and has daily coverage in the polar regions.
110   Over sea ice the first Stokes parameter, the average of the horizontally and the vertically polarized brightness temperatures, is
almost independent of incidence angle in range of 0°-40° and independent of both geometric and Faraday rotations, therefore,
robust to instrumental and geophysical errors (Camps et al., 2005). We average the intensities over the incidence angle range
of 0°-40° to reduce the uncertainty of single measurement. The daily averaged brightness temperature intensities in the Arctic
and in the Antarctic are interpolated with nearest neighbor algorithm and gridded into the National Snow and Ice Data Center
115   (NSIDC) polar stereographic projection with a grid resolution of 12.5 km. The southern and northern boundaries of the polar
regions are defined as latitude 50°N and 50°S for the sea-ice thickness retrieval. The L3B brightness temperatures are also
included in the SMOS L3C sea-ice thickness product.

2.1.2   JRA-55 reanalysis data

To estimate ice surface temperature, we extract the 2 m surface air temperature and the 10 m wind velocity data from JRA-55
120   atmospheric reanalysis (Kobayashi et al., 2015) and interpolate them using GMT surface command into the polar stereographic
projection with 12.5 km grid resolution (Wessel et al., 2019). JRA-55 reanalysis data provide various physical variables in 1.25°
resolution every six hours. For SMOS retrieval we consider three previous days temperature and wind field data and average
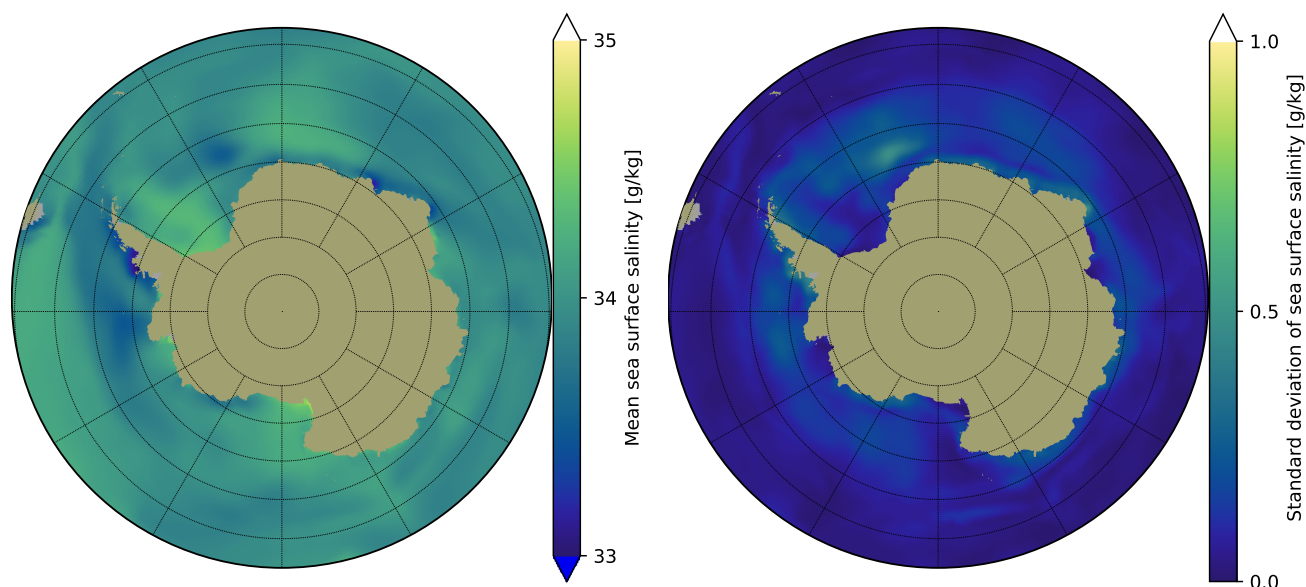
Figure 1. Mean (left) and standard deviation (right) of SSS in the Antarctic. The mean and standard deviation are calculated from monthly climatology. Note that the colorbars have different scales.

them as boundary conditions for a thermodynamic model. We assume in the thermodynamic model an immediate equilibrium at air-ice surface, therefore, the time average resembles a temperature diffusion process towards deeper emitting layers.

125   2.1.3   Sea surface salinity climatology

The Sea Surface Salinity (SSS) climatology in the Antarctic (Figure 1) is based on the monthly model outputs of GECCO2, a quasi-global simulation using MITgcm model over the years of 1952-2001. The model has a horizontal resolution of 1°x1°, with 23 vertical levels. Various in-situ measurements and satellite data are assimilated (Köhl and Stammer, 2008). In contrast to the highly variable SSS distribution in the Arctic due to river run-offs, SSS in the Antarctic is relatively constant, slightly

130   varying between 33-35 $\mathrm{g\,kg^{-1}}$, with a standard deviation less than 1 $\mathrm{g\,kg^{-1}}$.

2.2   Data used for the validation

In this study SMOS sea-ice thickness data are compared with HEM, SUIT, and ULS measurements conducted in the Weddell Sea.

2.2.1 Sea-ice thickness measured by HEM

135   Sea-ice thickness was measured using helicopter-based electromagnetic induction sounding (HEM) during one of the rare Polarstern Antarctic winter expeditions ANT-XXIX/6 in 2013. On four days (19, 20, and 21 June, 2013 and 7 July, 2013) measurements have been carried out in areas with first-year ice conditions. The flight track positions are shown in Figure 2. HEM measures the total thickness of snow and ice from the difference of electromagnetically determined ice/water interface and the laser-measured snow surface. The accuracy of HEM measurements is around 10 cm over level ice (Haas et al., 2009).

140   ### 2.2.2 Sea-ice thickness derived from ULS measurements

Upward-Looking Sonars (ULS) have been moored at diverse locations in the Weddell Sea and have measured the ice draft over various deployment periods between 1990-2010 (Behrendt et al., 2013; Behrendt et al., 2015). The uncertainty of the ULS ice draft measurements is between $\pm$ 5 cm to $\pm$ 23 cm depending on different correction methods (Behrendt et al., 2013). The opening angle of the acoustic beam results in a measurement footprint of approximately 6–8 m in diameter which is sampled 145   every 2-15 minutes depending on battery and data storage capacities (Behrendt et al., 2013). The total sea-ice thickness is derived from ice draft using the empirical relationship

$$z = 0.028 + 1.012d \tag{1}$$

where d is the sea-ice draft, and z is the total sea-ice thickness (Behrendt et al., 2015). Due to the large discrepancy between spatial resolution and sample coverage, it is necessary to compare ULS measurements with SMOS data over longer time peri-150   ods. A simple arithmetic average is used to calculate the mean values, using all available samples including open water. Three ULS sensors (AWI227, AWI229 and AWI231) have been deployed in areas of predominantly first-year ice and operated for a sufficiently long period of time (Table 1). The ULS AWI230 and AWI210 measured for more than two years in intermediate thick ice conditions and are also used for comparisons. Four ULS (AWI229, AWI206, AWI208, and AWI232) include data for the year 2010 and are therefore also used for a direct comparison to SMOS. The positions of all moorings are shown in Figure 155   2.

2.2.3 Sea-ice thickness derived from SUIT measurements

The Surface and Under-Ice Trawl (SUIT) was used to investigate the large-scale variability of physical and biological sea-ice properties during five campaigns in polar oceans (Castellani et al., 2019; Castellani et al., 2020). The Polarstern cruise PS81 was conducted during wintertime (August-October, 2013) in the marginal ice zone of the Weddell Sea and is therefore 160   suited for comparisons with the SMOS sea-ice thickness. The sensor array of the SUIT includes an altimeter (Tritech PA500/6-E) incorporated into a Conductivity Temperature Depth (CTD) probe. The sea-ice draft is derived by combining the depth measurements from the CTD pressure sensor with the distance from the sea-ice, and is then corrected with pitch and roll measurements from an Acoustic Doppler Current Profiler (ADCP). The total sea-ice thickness was derived by assuming a fixed

Table 1. Available ULS moorings used and neglected in this study. The maximum draft is the maximum of the averaged seasonal cycle calculated from monthly mean values.

ULS	Latitude [°]	Longitude [°]	Max. draft [m]	# Data [months]	year 2010
AWI227	-59.07	0.07	0.56	47	
AWI229	-63.97	-0.05	0.75	129	yes
AWI231	-66.51	-0.03	0.88	99	
AWI230	-66.01	0.17	0.99	32	
AWI210	-69.66	-15.71	1.71	25	
AWI206	-63.48	-52.10	2.79	56	yes
AWI208	-65.61	-37.41	1.72	54	yes
AWI232	-69.00	-0.00	2.01	141	yes
neglected					
AWI207	-63.71	-50.84	2.42	87	
AWI209	-66.62	-27.12	1.20	12	
AWI212	-70.91	-11.96	3.94	25	
AWI217	-64.42	-45.85	2.93	25	
AWI233	-69.39	-0.07	3.07	41	

density value ($\rho = 917\,\mathrm{kg\,m^{-3}}$) for sea ice and hydrostatic equilibrium. Figure 2 shows the positions of nine SUIT traverses of

165 different profile lengths ranging from 800 m to 3000 m.

3   SMOS sea-ice thickness retrieval algorithm

The retrieval algorithm is described in detail in (Tian-Kunze et al., 2014), in the following we summarize the basic principles. The SMOS sea-ice thickness is produced using an iterative retrieval algorithm that is based on a thermodynamic sea-ice model and a radiative transfer model (Figure 3), which takes variations of ice temperature and ice salinity into account. In

170 addition, ice thickness variations within the SMOS spatial resolution are considered through a statistical thickness distribution function derived from high-resolution ice thickness measurements from NASA's Operation IceBridge campaign (Tian-Kunze et al., 2014). This retrieval algorithm has been used to generate the operational Arctic SMOS sea-ice thickness product at Alfred-Wegener-Institute in the framework of "The SMOS and CryoSat-2 Sea Ice Data Product Processing and Dissemination Service", supported by ESA.

175 The measured SMOS brightness temperature depends on the ice concentration, the temperatures of the sea and the ice, and their emissivity. The sea ice emissivity depends on the sea ice microphysical structure but the inhomogeneities like brine
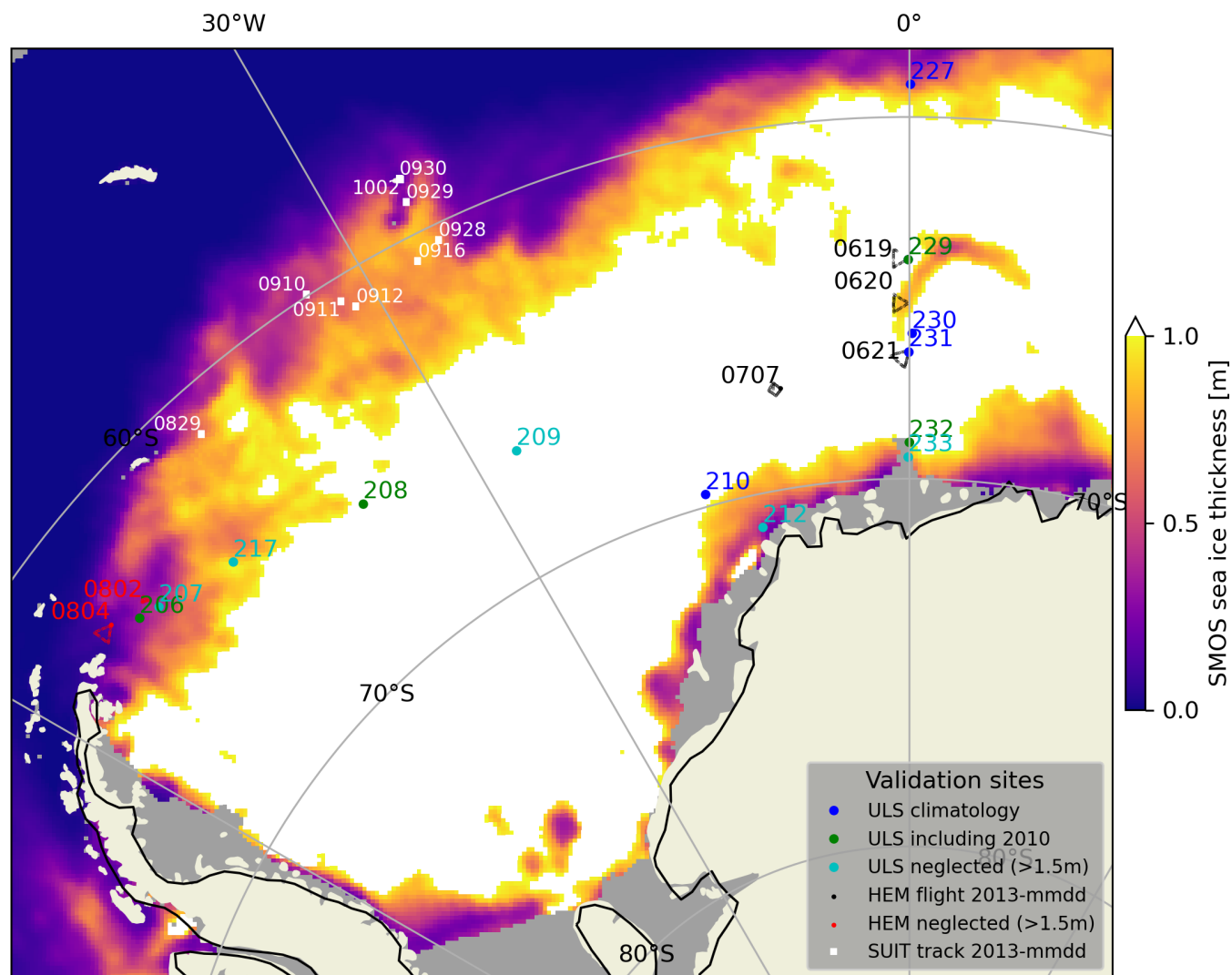
Figure 2. Overview of all available validation data used and neglected for the present study. The positions of ULS moorings, SUIT traverses and HEM flights are shown. The background shows the SMOS sea-ice thickness averaged for August 2010, a period where some ULS data are still available.

pockets and air bubbles are much smaller than the wavelength of 21 cm. Therefore, we can consider sea ice as a homogeneous medium and neglect volume scattering. The modelled sea ice emissivity used for the present retrieval mainly depends on ice thickness d_{ice}, ice temperature T_{ice}, and ice salinity S_{ice}. The retrieval consists of a simple one-layer radiation model (Menashi et al., 1993) and a thermodynamic model (Maykut, 1986). The radiation model calculates the emissivity of the sea ice layer and the underlying sea water. Brightness temperatures are derived from the emissivity and physical temperatures of sea ice and sea water. Because the emissivity is a function of T_{ice} and S_{ice}, the two parameters need to be estimated using auxiliary data.

Bulk ice salinity is estimated from sea surface salinity S_w using empirical relationship (Kovacs, 1996). S_w is extracted from Antarctic-wide SSS climatology that is derived from model output (Section 2.1.3).

185 We use bulk ice temperature T_{ice} as the physical sea ice temperature since we apply only one ice layer. The bulk ice temperature is estimated from the thermodynamic model, using auxiliary 2 m air temperature T_a and wind velocity u from atmospheric reanalysis data. Thermal equilibrium is assumed at the surface of the ice layer and the heat fluxes are calculated with a thermodynamic model based on Maykut (1986). Under the assumption of thermal equilibrium, the incoming and outgoing heat fluxes compensate each other (Figure 3).

190 The sea-ice thickness retrieval scheme is shown in Figure 4. The processing is performed in three steps:

1. An intermediate brightness temperature dataset L3A is generated from L1C data daily and saved in HDF file format on the local server. These files include all information provided in L1C swath data, but sorted by an equal-area grid (15 km, ISEA 4H9 grid, L1C data is provided on this grid) to ease the reading process of L1C swath files.

2. Gridded L3B brightness temperature data in NSIDC polar-stereographic projection with 12.5 km grid resolution are 195 generated from L3A data for the northern and southern hemisphere each.

3. L3C ice thickness is generated from L3B brightness temperatures using a pre-calculated look-up table, with JRA55 reanalysis and sea surface salinity climatology as auxiliary data.

The underestimation bias caused by the assumption of a 100% ice coverage increases with decreasing ice concentration (Tian-Kunze et al., 2014). An estimation of the retrieval bias and uncertainty has been carried out in a previous study (Tian-200 Kunze et al., 2014) in the Arctic. The attempt to correct the bias with ice concentration data from passive microwave radiometer data has revealed more problems due to the uncertainties in the ice concentration data itself. Tian-Kunze et al. (2014) has shown that in the regions with high concentrations, correcting the retrieved ice thickness with ice concentration data set with an uncertainty of 5% can cause higher errors than the 100% ice coverage assumption.

The thermodynamic insulation effect of snow is considered in the SMOS retrieval by using a simple statistical relation 205 between ice and snow thickness, i.e. that the snow depth on top of the sea ice is 10% of the sea-ice thickness. To estimate the total (snow+ice) sea-ice thickness 10% needs to be added to the SMOS sea-ice thickness included in the product. The additional snow is neglected in the following for the sake of simplicity except for one example (Tab. 2).

4 Antarctic SMOS Sea-ice Thickness Climatology

SMOS sea-ice thickness retrieval is suitable for thin ice detection, i.e. mostly thin first year ice. As ice grows, SMOS brightness 210 temperature gets saturated against ice thickness and the uncertainty increases exponentially with increasing ice thickness. For sea ice thicker than about 1 m, the algorithm only provides an estimate of the maximal retrievable ice thickness (Tian-Kunze et al., 2014). This leads to considerable underestimates of the thickness where the sea ice is thicker than one meter, e.g. in areas of deformed and multi-year ice.
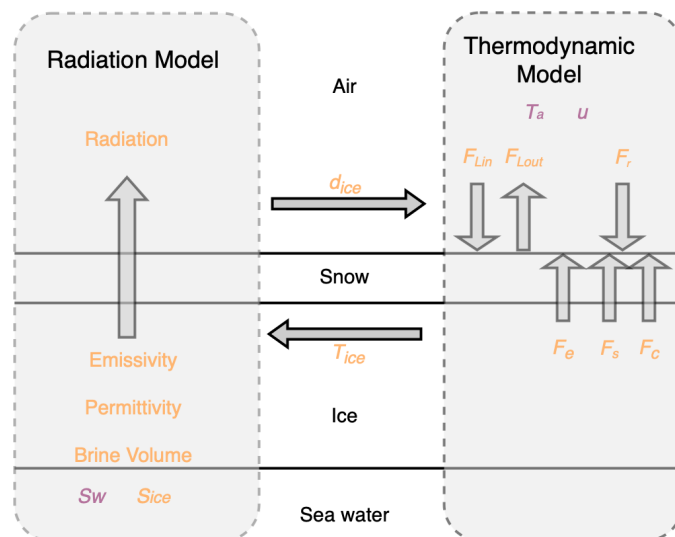
Figure 3. Retrieval structure with L-band brightness temperature radiation model and thermodynamic model. Variables in purple are input parameters from auxiliary data, in orange are the calculated parameters within the retrieval model. F_r is incoming shortwave radiation, F_{lin} and F_{lout} are incoming and outgoing longwave radiation, F_e, F_s, and F_c are latent heat flux, sensitive heat flux, and conductive heat flux respectively.

In addition, Antarctic ice drift causes frequent occurrence of leads due to ice divergence. The retrieval assumes 100% ice coverage which leads to an underestimation of the ice thickness in regions with significant fractions of open water like in the marginal ice zone. Nevertheless, the growth and distribution of the seasonal ice around Antarctica is well captured by SMOS. Figure 5 shows the monthly mean sea-ice thickness averaged over the time period of 2010 to 2023. Antarctic ice thickness, version v3.2, was only retrieved during austral winter periods, from 15 April to 15 October, therefore, for April and October only a half month is used to calculate the mean. The period was extended for version v3.3 to investigate the range of validity of the product.

Thick ice is observed throughout the seasons in the western Weddell Sea, where thick multiyear ice dominates. In the freeze-up period, both ice coverage and ice thickness increases rapidly around the Antarctic coast. Eastern Weddell Sea and Ross Sea show similar ice thickness conditions from fall to spring, with thick ice more dominant in winter, whereas in fall and spring considerably large areas of thin ice is present. In Western Pacific and Indian Ocean thin ice is dominant even in winter.

Around Antarctic coast there are frequent polynya openings due to katabatic winds. The SMOS retrieval demonstrates its advantage detecting polynya areas covered by thin ice (Figure 5).

The anomalies with respect to the total monthly means, the climatology, are shown in Fig. 6 for February to July 2023.
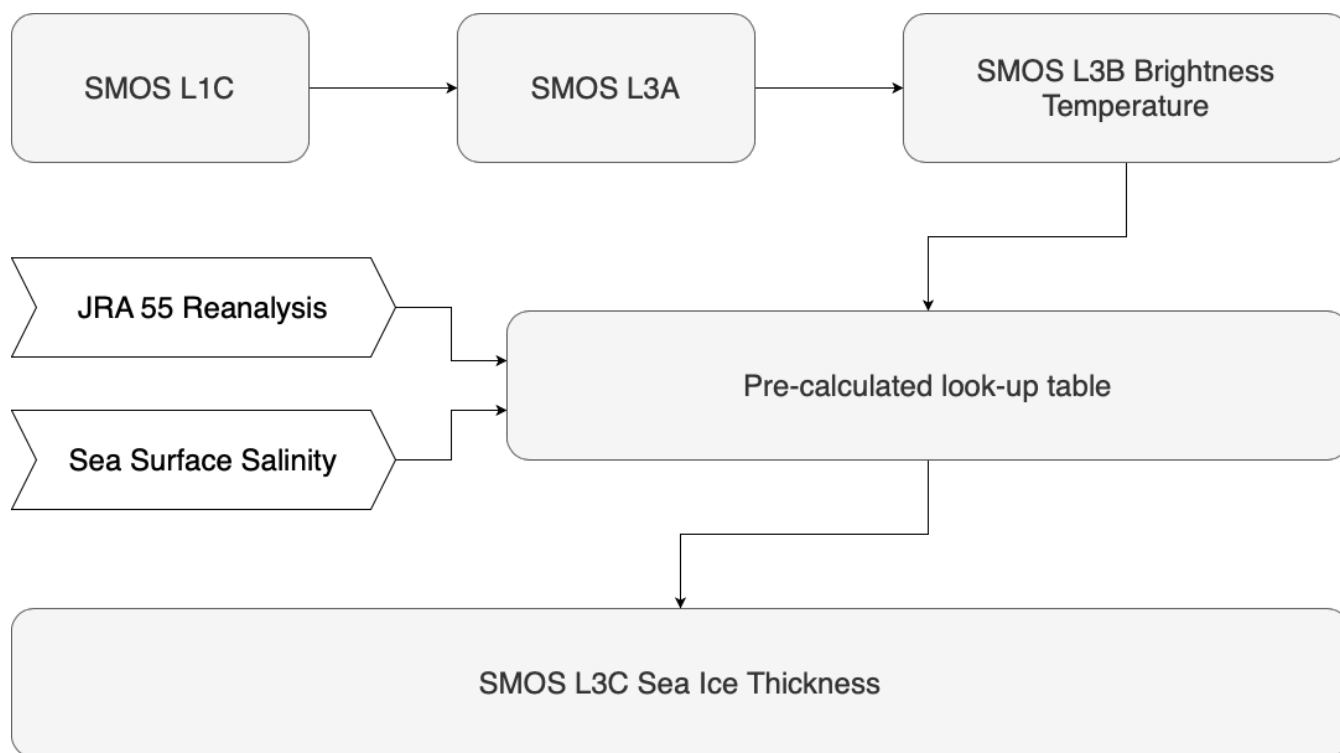
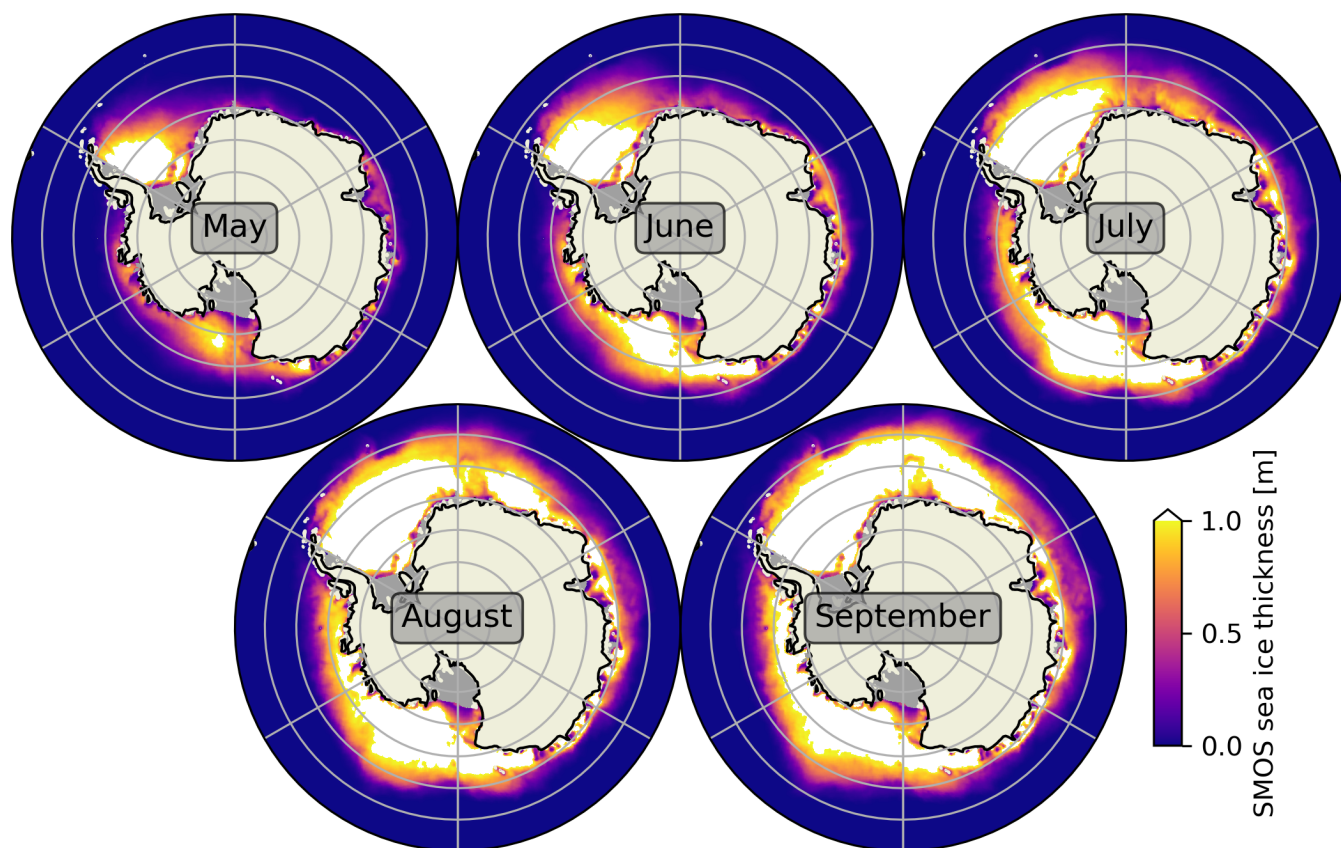**Figure 4.** Schematic flow chart of SMOS sea-ice thickness retrieval.

Figure 5. Average SMOS sea-ice thickness (version 3.3) over the time period of 2010-2023 from May to September.
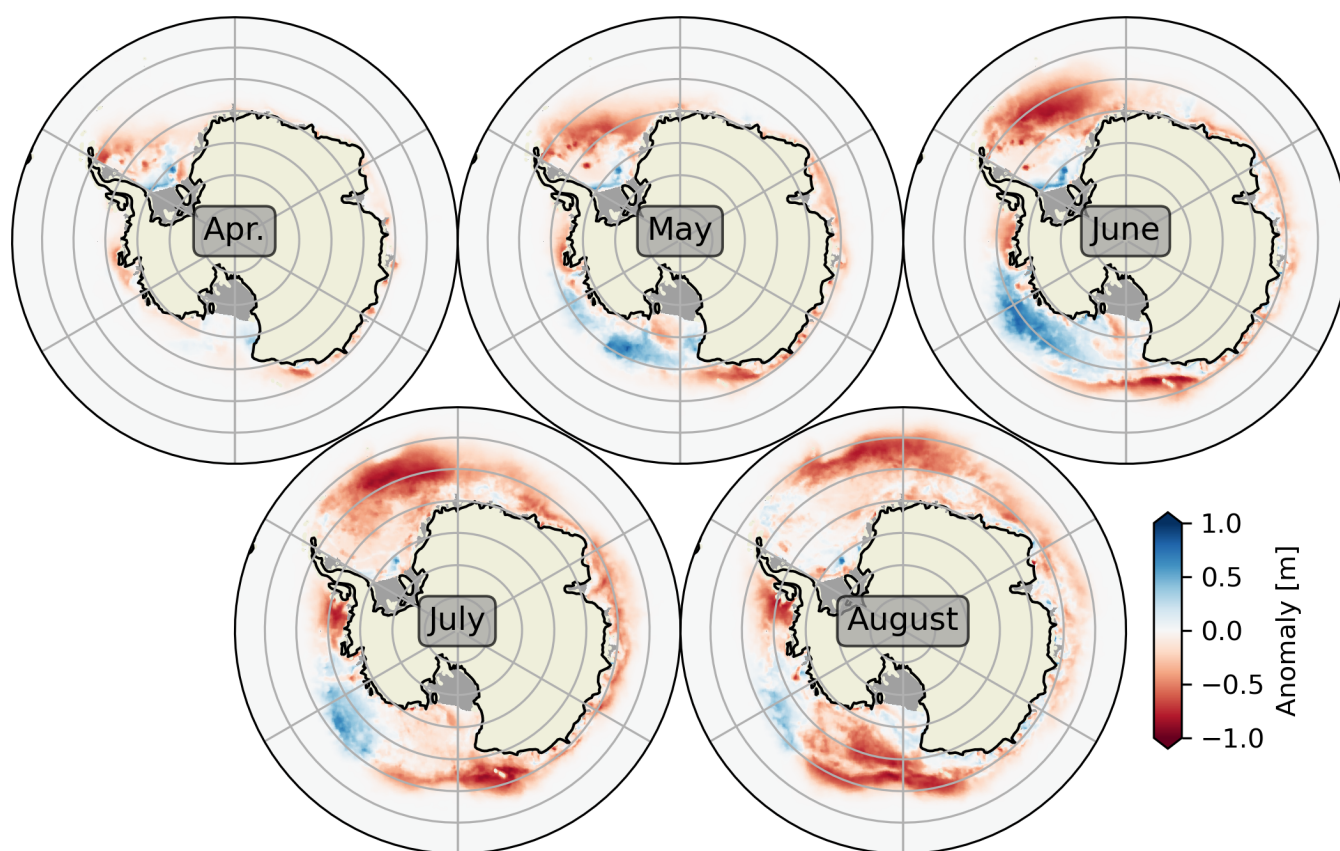
Figure 6. SMOS sea-ice thickness anomalies from April to August 2023 (monthly means, version 3.3). The reference period is from 2010-2023.

5 Validation

5.1 Validation with HEM measurements

230 Sea-ice thickness measurements using the HEM-method (Section 2.2.1) cover a spatial scale comparable to the SMOS radiometer resolution and therefore allow direct comparisons for specific days. Four measurement flights have been conducted in areas where the sea-ice thickness is within the valid range for the SMOS retrieval. The flight tracks are displayed in Figure 2 and summarized in Tab. 2 together with the SMOS sea-ice thickness for the two different versions v3.2 and v3.3. For the comparison, we take two different approaches, on the one hand based on individual SMOS pixels and on the other hand by
235 averaging over the entire flight tracks for the respective days. Although the grid used has a spatial sampling size of 12.5 km, the actual resolution of the SMOS radiometer footprint is significantly lower at about 35 km for nadir and coarser at other angles of incidence. Therefore, the individual SMOS pixels are not independent of each other, which justifies the approach of averaging over the entire flight.

The sea-ice thickness pattern from the four HEM flight tracks is well represented in the SMOS data, with the thinnest ice
240 (HEM average 0.52 m) detected on 19 June, 2013 at the southernmost location close to the prime meridian and the thickest ice (HEM average 1.33 m) observed on 7 July 2013 at about 9°W. The correlation coefficient R is 0.7 with a root mean square deviation of 0.26 m between two data sets for $N = 53$ individual SMOS pixels. Both versions v3.2 and v3.3 show similar results but v3.3 exhibits about 5 cm thicker ice and slightly increased RMSD.

Table 2 summarizes the metrics calculated for the averages over the four entire flights as well as for the single pixel. The
245 mean deviation is about 3 - 8 cm for both the pixel-based and flight-based approaches, while the root mean square deviation for the averaged flights reduces to 0.1 - 0.15 m and the correlation coefficient increases. A comparison with a 10% snow layer shows a significant additional deviation and increased RMSD. Based on this comparison to the HEM data we conclude, that the SMOS sea-ice thickness should rather be interpreted as the total (snow+ice) thickness.

5.2 Validation with SUIT measurements

250 With an average trawl distance of about 2 km the SUIT measurements sample only a small part of the SMOS measurement footprint and are therefore not representative for inhomogeneous ice conditions. Polarstern's cruise track can also lead to sample selection bias. The open water fraction about 10-20% derived from the SUIT zero thickness values is consistent with an overall reduced ice concentration in the marginal ice zone (not shown). This relatively large proportion of open water can explain the underestimation of the SMOS sea-ice thickness based on the assumption of a 100% ice cover. The underestimation
255 compared to the validation data is about 25 cm for the median of the SUIT tracks and 45 cm for the mean (Table 2). The differences between the SMOS sea-ice thickness versions v3.2 and v3.3 are negligible.

Table 2. Mean deviation (MD) and RMSD of SMOS and validation ice thicknesses in the Weddell Sea, 2013. All length units in cm. Two kind of validation data are used, HEM and SUIT. N is the number of co-located data points for the pixel-based comparison and for the averaged flights, respectively. R is the value of Pearson's correlation coefficient. The comparison v3.3+10% exemplifies the influence of the otherwise neglected snow.

Time period	Val.	$\mu\pm\sigma$	SMOS	$\mu\pm\sigma$	N	R	MD	RMSD
June-July	HEM	83±37	v3.2	85±25	53 pixels	0.71	2.8	26
June-July	HEM	83±37	v3.3	90±25	53 pixels	0.69	7.4	28
June-July	HEM	83±32	v3.2	86±23	4 flights	0.99	2.6	10
June-July	HEM	83±32	v3.3	91±22	4 flights	0.96	7.5	14
June-July	HEM	83±32	v3.3+10%	94±26	4 flights	0.96	17	20
Aug.-Oct.	SUIT mean	79±33	v3.2	34±16	9 pixels	0.66	-45	52
Aug.-Oct.	SUIT median	59±24	v3.2	34±16	9 pixels	0.71	-25	30
Aug.-Oct.	SUIT mean	79±33	v3.3	36±18	9 pixels	0.66	-43	50
Aug.-Oct.	SUIT median	59±24	v3.3	36±18	9 pixels	0.69	-23	29

5.3 Validation with ULS data

We group the ULS data in different sets. There are three ULS datasets (ULS set1, Table 3) that meet all selection criteria for a comparison (Section 2.2.2). ULS set2 includes one slightly shorter data set (AWI230), and set3 another one (AWI210) in a
260 region with thicker ice.

Since a direct comparison is not very meaningful due to the low representativeness of the point samples, we first compare the monthly climatologies. Another limitation is the mismatched time period for averaging which is 1996-2010 for the longest ULS dataset (AWI229) versus 2010-2020 for SMOS v3.2 and 2010-2023 for SMOS v3.3. If we assume a stationary climate, the monthly mean sea-ice thickness values and the interannual variability should still be comparable. In fact, there is reasonable
265 good agreement regarding the seasonal cycle (Figure 8) for the ULS within the valid thickness range. The ULS AWI210 measures too thick ice which is mostly outside the valid range for the SMOS retrieval.

The scatterplot (Figure 9) and the statistical metrics (Table 3) confirm the general validity. With a slight overestimation of 2-3 cm, SMOS is very close to the ULS measurements, also the interannual variability is very similar. The mean squared error can be given as 14 cm. With $N = 21$ monthly mean data points, a high correlation of $R = 0.94$ is achieved for v3.2 and with
270 $N = 36$ a correlation of $R = 0.95$ for ULS set2 and v3.3. Including the thicker ice ULS AWI210 (set3) shows the increased uncertainty of the retrieval for sea-ice thicker than about one meter.

A direct comparison of SMOS with ULS data for 2010 confirms the general picture. Fig. 10 shows the daily mean ULS sea-ice thickness together with values from the respective co-located SMOS pixel. Table 4 provides the corresponding statistics. In terms of mean deviation the best agreement can be seen with the ULS AWI229. However, this data set is also problematic due

Earth System
Science
Data
Open Access Discussions

Table 3. Mean deviation and RMSD of SMOS and ULS sea-ice thickness based on monthly long-term "climatological" mean. All length units in cm. ULS set1 consists of ULS 227, 229 and 231, set2 additionally includes ULS 230, and set3 ULS 210.

Time period	Val.	$\mu\pm\sigma$	SMOS	$\mu\pm\sigma$	N	R	MD	RMSD
Apr. - Oct.	ULS set1	46±32	v3.2	49±38	21	0.94	3	14
Feb. - Oct.	ULS set1	36±33	v3.3	38±40	27	0.97	2.3	12
Feb. - Oct.	ULS set2	38±36	v3.3	40±40	36	0.95	0.9	13
Feb. - Oct.	ULS set3	52±50	v3.3	46±43	45	0.91	-5.5	22

Table 4. Mean deviation and RMSD of SMOS and ULS sea-ice thickness based on the period of temporal overlap in 2010. All length units in cm.

Time period	Val.	$\mu\pm\sigma$	SMOS	$\mu\pm\sigma$	N	R	MD	RMSD
Feb. - Oct.	ULS 206	249±138	v3.3	34±27	213	0.34	-215	252
Feb. - Oct.	ULS 208	125±70	v3.3	74±46	214	0.68	-50	72
Feb. - Oct.	ULS 229	38±37	v3.3	45±53	164	0.75	6.4	36
Feb. - Oct.	ULS 232	103±68	v3.3	64±47	212	0.73	-40	51

275 to larger data gaps in the ULS record. A very good general agreement can be seen regarding the presence of ice, which is also accompanied by relatively high correlation coefficients.

6 SMOS regional sea-ice extent compared with independent passive microwave data

This section discusses how to check the general quality and completeness of the SMOS sea-ice thickness product. For this purpose, a regional extent parameter derived from SMOS is compared with independent standard sea-ice extent products,
280 hereinafter referred to as reference. In the following we use the NSIDC sea-ice index derived from the Special Sensor Microwave Imager/Sounder (SSMIS) and a regional mask from longitudinal boundaries (Meier et al., 2007, 2022). The SMOS sea-ice (thickness) extent is defined as the area covered by all pixels above a threshold thickness of $h_0 = 3\,\text{cm}$ (Kaleschke and Tian-Kunze, 2021). By assuming the reference product is of high quality and consistency, the difference between the sea-ice extent values can measure the quality and consistency of the SMOS sea-ice product. The advantage of the method is the similar
285 spatial resolution and temporal sampling of both independent sensors which allows to identify significant deviations from a mean quality in terms of completeness and consistency.

The plot in Figure 11 allows the quality control in a visual way. The overall consistency is very good and confirms the high quality of the SMOS sea-ice data. Significant deviations can be seen only very seldom with the exception of the first months due to the SMOS in-orbit commissioning phase in early 2010 (Martín-Neira et al., 2016). The negative deviations, viewed
290 as downward spikes relative to the reference, are almost always related to missing data shown on the same chart. same plot.

Missing data occurs mostly over the open ocean and not within sea ice and can for example be caused by RFI from radio sources on vessels, or just result from gaps between the orbital swaths. However, the Antarctic is of course much cleaner with respect to RFI sources compared to the populated Northern Hemisphere Furthermore, we do see an improvement from version v3.2 to v3.3 which is related to changes in the underlying SMOS L1C brightness temperature data v724 compared to

295 the previous operational version v620. All deviations are negative, in line with the reason of missing data, with one exception for May 27, 2017 and version v3.2. This positive deviation, visible as an upward spike relative to the reference, is caused by corrupted data, a processing artefact, which was unfortunately not detected before the submission of the data to the Pangaea archive. The new version v3.3 is not affected.

The final graph Fig 12 shows the total sea-ice extent for the beginning of month from 2010 to 2023. A very good general

300 agreement between the reference and SMOS extent can be seen. Furthermore, in both time series, the decrease and record lows since the year 2021 are noteworthy.

In summary, the quality control confirms the good quality of the SMOS sea ice data relative to the reference. The first few months of 2010 should be treated with care because of effects from the satellite commissioning phase. In general, rare data gaps could easily be filled with interpolated data if necessary. SMOS sea-ice thickness data version v3.3 supersedes v3.2 with

305 better quality in terms of completeness but otherwise with no notable differences.

7 Discussion

SMOS sea-ice thickness in the Antarctic is still a preliminary product with lots of room for improvement. Although it is here derived using the same retrieval algorithm as in the Arctic, the situation in the Antarctic is more complicated and uncertain. This is due to various influencing factors. First, due to Antarctica's remote location and lack of commercial exploitation, there

310 have been fewer applications for Antarctic sea-ice thickness. As a result, there is much less observational, in situ, and validation data. Second, the sea-ice conditions are different than in the Arctic and it is unclear how the retrieval procedure needs to be adjusted, e.g. more snow and flooding. Third, this also affects other remote sensing methods and therefore there is much less data to compare. In this first analysis we only compare the SMOS data based on the resulting sea-ice thickness. Further analyses regarding the validity of sea-ice physics and retrieval parameterisations have yet to follow. Sea-ice thickness validation is not

315 universal due to the limitations of SMOS retrieval. The existence of an upper limit for the sea-ice thickness retrieval requires a range selection of the validation data with a maximum of about one meter. It is not possible to decide whether the sea ice is thicker than one meter based on the SMOS data alone. The scope of application of the SMOS data is therefore in areas with thin sea ice or in synergetic combination with altimeters. Due to a pre-selection of suitable validation data, only the application for the area of thin sea ice is considered here. An important characteristic of the validation data is its representativity in the SMOS

320 footprint. While the helicopter can measure hundreds of kilometers, the SUIT's use is limited to distances of a few kilometers and thus only captures a small fraction of a SMOS footprint with a diameter of around 35-40 km. It is therefore not surprising that the comparison with the SUIT data showed the worst agreement with the SMOS sea-ice thickness. The underestimation at the sea-ice margin is likely to be a real deficit at least in this specific area where relatively thick sea ice is drifting out of

the Weddell sea. Little can be done about this problem unless additional sensors are used at the same time to correct for the

325   influence of sea ice concentration. One basic assumption for the sea-ice thickness retrieval is a closed ice coverage (100% sea ice concentration) (Tian-Kunze et al., 2014). This assumption often does not hold in the divergent marginal ice zone where the SUIT measurements were conducted. In summary, the SUIT measurements show a substantial underestimation of the SMOS sea-ice thickness and the current method is not suitable for capturing this uncertainty. However, since the representativeness of the SUIT measurements is low, these results are not given much significance in the overall assessment.

330   The HEM flights and ULS measurements are much more representative since they cover larger fractions of the SMOS footprint and longer time periods, respectively. Based on averaged HEM flights and monthly ULS climatologies we find a small mean difference (bias) of less than 3 cm and root-mean-square deviation of about 15 cm with a high correlation coefficient $R>0.9$ for the valid sea-ice thickness range between zero and about one meter. This results gives us good confidence in the overall validity of the SMOS dataset for thin sea ice. In the present version, the SMOS sea-ice thickness should be considered

335   as the total (snow+ice) thickness for the best agreement with the validation reference.

However, there are some issues that are not captured by the validation at just a few sites. One obvious artefact which can be seen in the SMOS climatologies (Figures 2 and 5) is the persistent relatively small sea-ice thickness at about 75.3°S, 37.3°W in the Weddell Sea in front of the Filchner-Ronne ice shelf. This is the position of the iceberg A-23A (e.g. Paul et al., 2015), which was the largest iceberg in the world until A-76 took over that title in 2021. Icebergs are transparent at L-band frequency

340   due to the very large penetration depth in their almost salt-free ice of meteoric origin (Giovanni et al., 2017). Therefore, huge icebergs correspond to low brightness temperatures and thus cause an incorrect small sea-ice thickness in the SMOS retrieval. If these icebergs are mostly stationary like A-23A, then they could be masked out which is not that simple with a static mask if they move. Similar problems exist with the coastal land mask used in the product, which is deprecated in some ice shelf areas. Theses effect has not yet been taken into account in the current SMOS sea-ice thickness product version and users should be

345   aware about these artefacts.

8   Conclusions

This paper presents the SMOS level 3 sea-ice thickness product and its initial validation for the Southern Ocean. The SMOS sea-ice thickness version v3.2 is based on the level 1C brightness temperature product version v620 and covers the years 2010 to 2020 during southern winter (defined here as from 15th April to 15th October). The updated product version v3.3 is based

350   on the L1C v724 and contains also the most recent data, including the exceptional 2023 anomaly. The processing period of v3.3 starts two months earlier although the data should be used with caution.

We selected three validation datasets from the Weddell Sea that have different degrees of representativeness: Helicopter-based EM Bird (HEM), Surface and Under-Ice Trawl (SUIT), and stationary Upward-Looking Sonars (ULS). Based on averaged HEM flights and monthly ULS climatologies we find a small mean difference (bias) and root-mean-square deviation of

355   about 30 cm with a high correlation coefficient $R>0.9$ for the valid sea-ice thickness range up to about one meter. We conclude

that the overall validity of the SMOS sea-ice thickness has been demonstrated for thin sea ice up to about 1 m thick. However, compared to measurements outside the valid thickness range, a strong underestimation can be observed.

Certain limitations of the present SMOS sea-ice thickness product need to be considered:

1. With SMOS data alone one can not provide an upper-limit estimate of the sea-ice thickness. This requires the combination with other sensors such as altimeters. More work is necessary to provide a combined synergy product that covers the full thickness range.

2. The assumption of fully closed sea-ice coverage (100% sea-ice concentration) is often not met, leading to a systematic underestimation of sea-ice thickness, especially in areas of ice divergence, such as within the marginal ice zone.

3. The SMOS sea-ice thickness v3.3 should be taken as the total sea-ice thickness, i.e. snow + ice thickness.

4. Icebergs are not flagged and show up as relatively thin sea ice in the product. Likewise, the shelf ice edge is not always up to date.

5. Apart from the auxiliary data, the present SMOS sea-ice thickness retrieval algorithm was not adapted for the Antarctic. Thus, there is room for improvement to optimize the method for Antarctic sea-ice conditions.

6. More representative sea-ice thickness measurements are needed for validation.

9   Code and data availability

The daily Antarctic SMOS sea-ice thickness data version 3.2 presented here can be assessed on the PANGAEA open data repository https://doi.org/10.1594/PANGAEA.934732 (Tian-Kunze and Kaleschke, 2021). The currently operational SMOS sea-ice thickness data version 3.3 are available through ftp://ftp.awi.de/sea_ice/product/smos/v3.3/sh/ and (soon) through the ESA dissemination server https://smos-diss.eo.esa.int/oads/access/collection/L3_SIT_Open. The basis for the SMOS sea-ice thickness data is the SMOS L1C brightness temperature product https://doi.org/10.57780/SM1-e20cf57. The ULS data are available from https://doi.org/10.1594/PANGAEA.785565 (Behrendt et al., 2013), SUIT data are available from https://doi.org/10.1594/PANGAEA.902334 (Castellani et al., 2019), HEM data are available from https://doi.org/10.1594/PANGAEA.944879 (Hendricks et al., 2022), JRA55 reanalysis data can be downloaded from https://rda.ucar.edu/data/ (Kobayashi et al., 2015), sea surface salinity data can be obtained from https://www.cen.uni-hamburg.de/icdc (Köhl and Stammer, 2008). The NSIDC regional sea ice index is available at https://nsidc.org/data/g02135.

Python/Jupyter notebooks to reproduce all figures and statistics are available on the AWI Gitlab repository: https://gitlab.awi.de/public_repository/smos_derived_antarctic_thin_seaice_thickness (a doi will be provided for the final version).

Open Access Earth System Science Data Discussions

References

390

Allan, R. P., Hawkins, E., Bellouin, N., and Collins, B.: IPCC, 2021: Summary for Policymakers, 2021.

Behrendt, A., Dierking, W., Fahrbach, E., and Witte, H.: Sea ice draft measured by upward looking sonars in the Weddell Sea (Antarctica), https://doi.org/10.1594/PANGAEA.785565, supplement to: Behrendt, A et al. (2013): Sea ice draft in the Weddell Sea, measured by upward looking sonars. Earth System Science Data, 5(1), 209-226, https://doi.org/10.5194/essd-5-209-2013, 2013.

395 Behrendt, A., Dierking, W., and Witte, H.: Thermodynamic sea ice growth in the central Weddell Sea, observed in upward-looking sonar data, Journal of Geophysical Research: Oceans, 120, 2270–2286, 2015.

Belter, H. J., Krumpen, T., Hendricks, S., Hoelemann, J., Janout, M. A., Ricker, R., and Haas, C.: Satellite-based sea ice thickness changes in the Laptev Sea from 2002 to 2017: comparison to mooring observations, The Cryosphere, 14, 2189–2203, 2020.

Camps, A., Vall-llossera, M., Batres, L., Torres, F., Duffo, N., and Corbella, I.: Retrieving sea surface salinity with multiangular L-band brightness temperatures: Improvement by spatiotemporal averaging, RADIO SCIENCE, 40, https://doi.org/10.1029/2004RS003040, 2005.

Castellani, G., Flores, H., Lange, B. A., Schaafsma, F. L., Ehrlich, J., David, C. L., van Franeker, J. A., Meijboom, A., van Dorssen, M., Vortkamp, M., and Van de Putte, A. P.: Sea ice draft, under-ice irradiance and radiance, and surface water temperature, salinity and chlorophyl a from Surface and Under Ice Trawl (SUIT) measurements in 2012-2017, https://doi.org/10.1594/PANGAEA.902056, 2019.

405 Castellani, G., Schaafsma, F. L., Arndt, S., Lange, B. A., Peeken, I., Ehrlich, J., David, C., Ricker, R., Krumpen, T., Hendricks, S., et al.: Large-scale variability of physical and biological sea-ice properties in polar oceans, Frontiers in Marine Science, p. 536, https://doi.org/https://doi.org/10.3389/fmars.2020.00536, 2020.

Eicken, H., Fischer, H., and Lemke, P.: Effects of the snow cover on Antarctic sea ice and potential modulation of its response to climate change, Annals of Glaciology, 21, 369–376, https://doi.org/10.3189/S0260305500016086, 1995.

410 Fons, S., Kurtz, N. T., Bagnardi, M., Petty, A. A., and Tilling, R.: Assessing CryoSat-2 Antarctic Snow Freeboard Retrievals Using Data From ICESat-2, Earth and Space Science, 8, e2021EA001 728, 2021.

Giles, K. A., Laxon, S. W., and Worby, A. P.: Antarctic sea ice elevation from satellite radar altimetry, Geophysical Research Letters, 35, 2008.

Giovanni, M., Francesco, M., Marco, B., Marion, L.-L., Niels, S., Steen, K., Rene, F., Ghislain, P., Lars, K., Andreas, W., and Arnaud, 415 M.: CryoSMOS -- Support To Science Elements SMOS+Cryosphere - Final Report - ESRIN Contract No. 4000112262/14/I--NB, https://doi.org/10.5281/zenodo.3406182, 2017.

Gómez-Valdivia, F., Holland, P. R., Siahaan, A., Dutrieux, P., and Young, E.: Projected West Antarctic Ocean Warming Caused by an Expansion of the Ross Gyre, Geophysical Research Letters, 50, e2023GL102 978, https://doi.org/https://doi.org/10.1029/2023GL102978, e2023GL102978 2023GL102978, 2023.

420 Haas, C., Lobach, J., Hendricks, S., Rabenstein, L., and Pfaffling, A.: Helicopter-borne measurements of sea ice thickness, using a small and lightweight, digital EM system, Journal of Applied Geophysics, 67, 234 – 241, https://doi.org/http://dx.doi.org/10.1016/j.jappgeo.2008.05.005, airborne Geophysics, 2009.

Hendricks, S., Hunkeler, P. A., and Schwegmann, S.: Airborne sea ice plus snow thickness in the Weddell Sea from Polarstern cruise PS81 (ANT-XXIX/6) in 2013, https://doi.org/10.1594/PANGAEA.944879, 2022.

425 Holland, P. R., Bruneau, N., Enright, C., Losch, M., Kurtz, N. T., and Kwok, R.: Modeled trends in Antarctic sea ice thickness, Journal of Climate, 27, 3784–3801, 2014.

Huntemann, M., Heygster, G., Kaleschke, L., Krumpen, T., Mäkynen, M., and Drusch, M.: Empirical sea ice thickness retrieval during the freeze-up period from SMOS high incident angle observations, The Cryosphere, 8, 439–451, https://doi.org/10.5194/tc-8-439-2014, 2014.

Kacimi, S. and Kwok, R.: The Antarctic sea ice cover from ICESat-2 and CryoSat-2: freeboard, snow depth, and ice thickness, The Cryosphere, 14, 4453–4474, 2020.

Kaleschke, L. and Tian-Kunze, X.: SMOS Sea Ice Thickness Data Product Quality Control by Comparison with the Regional Sea Ice Extent, in: 2021 IEEE International Geoscience and Remote Sensing Symposium IGARSS, pp. 1110–1113, https://doi.org/10.1109/IGARSS47720.2021.9553630, 2021.

Kaleschke, L., Tian-Kunze, X., Maaß, N., Mäkynen, M., and Drusch, M.: Sea ice thickness retrieval from SMOS brightness temperatures during the Arctic freeze-up period, Geophysical Research Letters, 39, https://doi.org/10.129/2012GL050916, 2012.

Kaleschke, L., Tian-Kunze, X., Maaß, N., Beitsch, A., Wernecke, A., Miernecki, M., Müller, G., Fock, B. H., Gierisch, A. M., Schlünzen, K. H., et al.: SMOS sea ice product: Operational application and validation in the Barents Sea marginal ice zone, Remote sensing of environment, 180, 264–273, 2016.

Kern, S. and Spreen, G.: Uncertainties in Antarctic sea-ice thickness retrieval from ICESat, Annals of Glaciology, 56, 107–119, 2015.

Kern, S., Ozsoy-Çiçek, B., and Worby, A. P.: Antarctic sea-ice thickness retrieval from ICESat: inter-comparison of different approaches, Remote Sensing, 8, 538, 2016.

Kerr, Y. H., Waldteufel, P., Wigneron, J. P., Martinuzzi, J., Font, J., and Berger, M.: Soil moisture retrieval from space: the Soil Moisture and Ocean Salinity (SMOS) mission, IEEE Transactions on Geoscience and Remote Sensing, 39, 1729–1735, https://doi.org/10.1109/36.942551, 2001.

Kobayashi, S., Ota, Y., Harada, Y., Ebita, A., Moriya, M., Onoda, H., Onogi, K., Kamahori, H., Kobayashi, C., Endo, H., et al.: The JRA-55 reanalysis: general specifications and basic characteristics, Journal of the Meteorological Society of Japan. Ser. II, 93, 5–48, 2015.

Köhl, A. and Stammer, D.: Variability of the meridional overturning in the North Atlantic from the 50-year GECCO state estimation, Journal of Physical Oceanography, 38, 1913–1930, 2008.

Kovacs, A.: Sea ice. Part 1, Bulk salinity versus ice floe thickness, 1996.

Kurtz, N., Studinger, M., Harbeck, J., Onana, V., and Farrell, S.: IceBridge Sea Ice Freeboard, Snow Depth, and Thickness., online, boulder, Colorado USA: NASA DAAC at NSIDC, 2012.

Laxon, S. W., Giles, K. A., Ridout, A. L., Wingham, D. J., Willatt, R., Cullen, R., Kwok, R., Schweiger, A., Zhang, J., Haas, C., Hendricks, S., Krishfield, R., Kurtz, N., Farrell, S., and Davidson, M.: CryoSat-2 estimates of Arctic sea ice thickness and volume, Geophysical Research Letters, 40, 732–737, https://doi.org/10.1002/grl.50193, 2013.

Li, Q., England, M. H., Hogg, A. M., Rintoul, S. R., and Morrison, A. K.: Abyssal ocean overturning slowdown and warming driven by Antarctic meltwater, Nature, 615, 841–847, https://doi.org/https://doi.org/10.1038/s41586-023-05762-w, 2023.

Maaß, N., Kaleschke, L., Tian-Kunze, X., Mäkynen, M., Drusch, M., Krumpen, T., Hendricks, S., Lensu, M., Haapala, J., and Haas, C.: Validation of SMOS sea ice thickness retrieval in the northern Baltic Sea, Tellus A: Dynamic meteorology and oceanography, 67, 24 617, https://doi.org/10.3402/tellusa.v67.24617, 2015.

Martín-Neira, M., Oliva, R., Corbella, I., Torres, F., Duffo, N., Durán, I., Kainulainen, J., Closa, J., Zurita, A., Cabot, F., Khazaal, A., Anterrieu, E., Barbosa, J., Lopes, G., Tenerelli, J., Díez-García, R., Fauste, J., Martín-Porqueras, F., González-Gambau, V., Turiel, A., Delwart, S., Crapolicchio, R., and Suess, M.: SMOS instrument performance and calibration after six years in orbit, Remote Sensing of Environment, 180, 19–39, https://doi.org/https://doi.org/10.1016/j.rse.2016.02.036, special Issue: ESA's Soil Moisture and Ocean Salinity Mission - Achievements and Applications, 2016.

465 Maykut, G.: Geophysics of Sea Ice, chap. The surface heat and mass balance, 395–463, 1986.

Mecklenburg, S., Drusch, M., Kaleschke, L., Rodriguez-Fernandez, N., Reul, N., Kerr, Y., Font, J., Martin-Neira, M., Oliva, R., Daganzo-Eusebio, E., Grant, J., Sabia, R., Macelloni, G., Rautiainen, K., Fauste, J., de Rosnay, P., Munoz-Sabater, J., Verhoest, N., Lievens, H., Delwart, S., Crapolicchio, R., de la Fuente, A., and Kornberg, M.: ESA's Soil Moisture and Ocean Salinity mission: From science to operational applications, Remote Sensing of Environment, pp. –, https://doi.org/http://dx.doi.org/10.1016/j.rse.2015.12.025, 2016.

470 Meier, W. N., Stroeve, J., and Fetterer, F.: Whither Arctic sea ice? A clear signal of decline regionally, seasonally and extending beyond the satellite record, Annals of Glaciology, 46, 428–434, https://doi.org/10.3189/172756407782871170, 2007.

Meier, W. N., Hovelsrud, G. K., Van Oort, B. E., Key, J. R., Kovacs, K. M., Michel, C., Haas, C., Granskog, M. A., Gerland, S., Perovich, D. K., et al.: Arctic sea ice in transformation: A review of recent observed changes and impacts on biology and human activity, Reviews of Geophysics, 52, 185–217, 2014.

475 Meier, W. N., Stewart, J. S., Windnagel, A., and Fetterer, F. M.: Comparison of Hemispheric and Regional Sea Ice Extent and Area Trends from NOAA and NASA Passive Microwave-Derived Climate Records, Remote Sensing, 14, https://doi.org/10.3390/rs14030619, 2022.

Menashi, J. D., St. Germain, K. M., Swift, C. T., Comiso, J. C., and Lohanick, A. W.: Low-frequency passive-microwave observations of sea ice in the Weddell Sea, Journal of Geophysical Research: Oceans, 98, 22 569–22 577, https://doi.org/10.1029/93JC02058, 1993.

Parkinson, C. L. and Cavalieri, D. J.: Antarctic sea ice variability and trends, 1979–2010, The Cryosphere, 6, 871–880, 2012.

480 Paul, S., Willmes, S., and Heinemann, G.: Long-term coastal-polynya dynamics in the southern Weddell Sea from MODIS thermal-infrared imagery, The Cryosphere, 9, 2027–2041, 2015.

Ricker, R., Hendricks, S., Helm, V., Skourup, H., and Davidson, M.: Sensitivity of CryoSat-2 Arctic sea-ice freeboard and thickness on radar-waveform interpretation, The Cryosphere, 8, 1607–1622, https://doi.org/10.5194/tc-8-1607-2014, 2014.

Ricker, R., Hendricks, S., Kaleschke, L., Tian-Kunze, X., King, J., and Haas, C.: A weekly Arctic sea-ice thickness data record from merged
485 CryoSat-2 and SMOS satellite data, The Cryosphere, 11, 1607–1623, https://doi.org/10.5194/tc-11-1607-2017, 2017.

Stammerjohn, S. and Maksym, T.: Gaining (and losing) Antarctic sea ice: variability, trends and mechanisms, in: Sea Ice, chap. 10, pp. 261–289, John Wiley & Sons, Ltd, https://doi.org/https://doi.org/10.1002/9781118778371.ch10, 2017.

Stroeve, J. C., Serreze, M. C., Holland, M. M., Kay, J. E., Malanik, J., and Barrett, A. P.: The Arctic's rapidly shrinking sea ice cover: a research synthesis, Climatic change, 110, 1005–1027, 2012.

490 Tian-Kunze, X. and Kaleschke, L.: SMOS-derived sea ice thickness in the Antarctic from 2010 to 2020, https://doi.org/10.1594/PANGAEA.934732, 2021.

Tian-Kunze, X., Kaleschke, L., Maaß, N., Mäkynen, M., Serra, N., Drusch, M., and Krumpen, T.: SMOS-derived thin sea ice thickness: algorithm baseline, product specifications and initial verification, The Cryosphere, 8, 997–1018, https://doi.org/10.5194/tc-8-997-2014, 2014.

495 Voosen, P.: Dwindling sea ice may speed melting of Antarctic glaciers, Science, pp. 118–119, https://doi.org/10.1126/science.adi2227, 2023.

Wessel, P., Luis, J. F., Uieda, L., Scharroo, R., Wobbe, F., Smith, W. H. F., and Tian, D.: The Generic Mapping Tools Version 6, Geochemistry, Geophysics, Geosystems, 20, 5556–5564, https://doi.org/https://doi.org/10.1029/2019GC008515, 2019.

Wever, N., Leonard, K., Maksym, T., White, S., Proksch, M., and Lenaerts, J. T.: Spatially distributed simulations of the effect of snow on mass balance and flooding of Antarctic sea ice, Journal of Glaciology, 67, 1055–1073, 2021a.

500 Wever, N., Leonard, K., Maksym, T., White, S., Proksch, M., and Lenaerts, J. T. M.: Spatially distributed simulations of the effect of snow on mass balance and flooding of Antarctic sea ice, Journal of Glaciology, 67, 1055–1073, https://doi.org/10.1017/jog.2021.54, 2021b.

Earth System
Science
Data

Worby, A. P., Geiger, C. A., Paget, M. J., Van Woert, M. L., Ackley, S. F., and DeLiberty, T. L.: Thickness distribution of Antarctic sea ice, Journal of Geophysical Research: Oceans, 113, 2008.

Xu, Y., Li, H., Liu, B., Xie, H., and Ozsoy-Cicek, B.: Deriving Antarctic Sea-Ice Thickness From Satellite Altimetry and Estimating Consistency for NASA's ICESat/ICESat-2 Missions, Geophysical Research Letters, 48, e2021GL093 425, https://doi.org/https://doi.org/10.1029/2021GL093425, e2021GL093425 2021GL093425, 2021.

Zhang, J.: Increasing Antarctic sea ice under warming atmospheric and oceanic conditions, Journal of Climate, 20, 2515–2529, 2007.

Zhou, S., Meijers, A. J., Meredith, M. P., Abrahamsen, E. P., Holland, P. R., Silvano, A., Sallée, J.-B., and Østerhus, S.: Slowdown of Antarctic Bottom Water export driven by climatic wind and sea-ice changes, Nature Climate Change, https://doi.org/https://doi.org/10.1038/s41558-023-01695-4, 2023.

Zwally, H. J., Yi, D., Kwok, R., and Zhao, Y.: ICESat measurements of sea ice freeboard and estimates of sea ice thickness in the Weddell Sea, Journal of Geophysical Research: Oceans, 113, 2008.
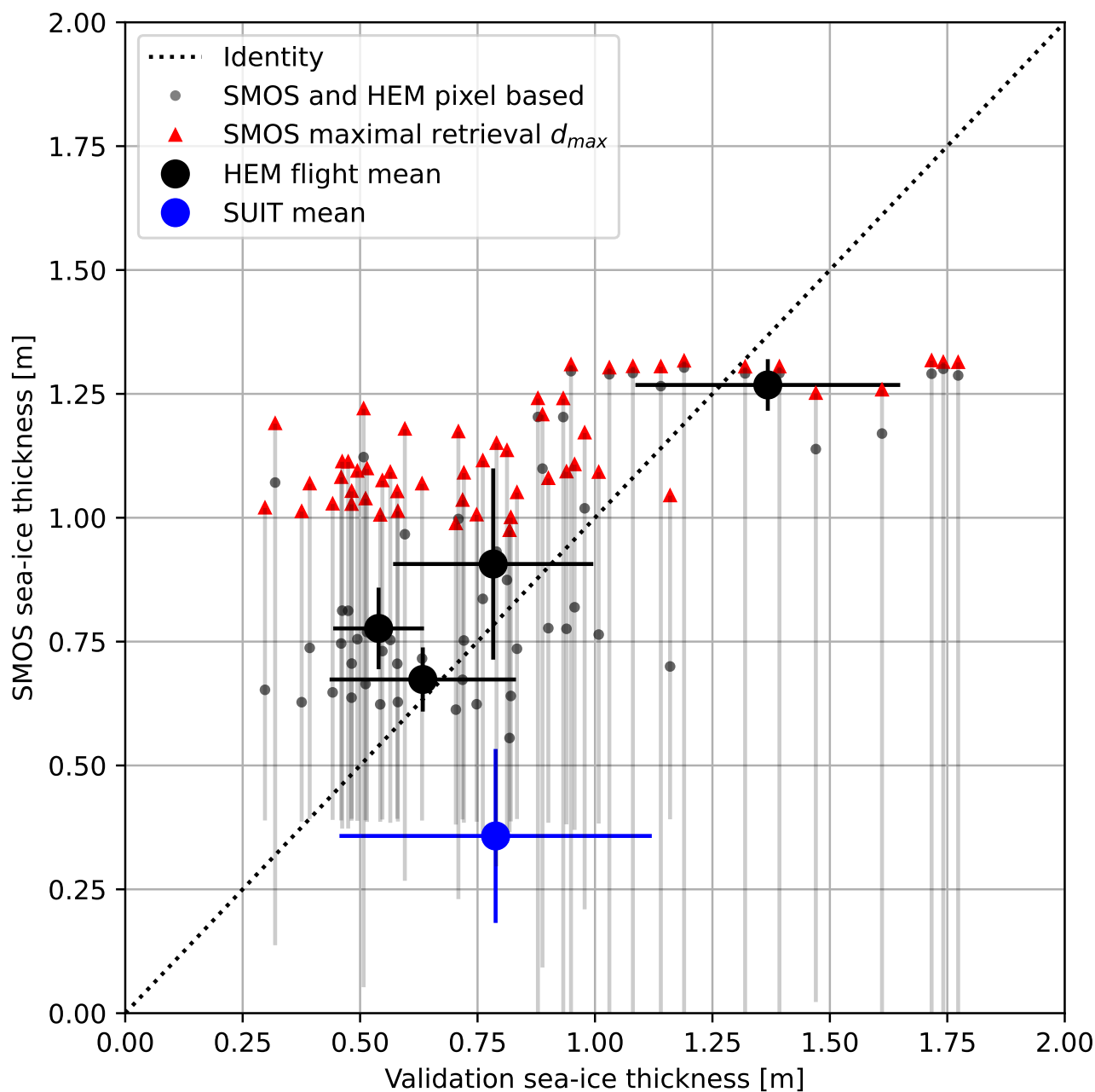
Figure 7. Scatter plot of SMOS sea-ice thickness and validation data collected in 2013. The graph includes airborne HEM (June/July) and underwater SUIT (Aug-October) thickness data for comparison. The maximum retrievable SMOS thickness is indicated with red triangles for pixel based data points (HEM only). The SMOS uncertainty as provided in the product is given by the lower y-error-bar. The big dots represent the averages over the entire flights and the error-bars their corresponding standard deviation. For SUIT the average over the entire set of measurements is shown with the standard deviation calculated from the averages of 9 tracks.
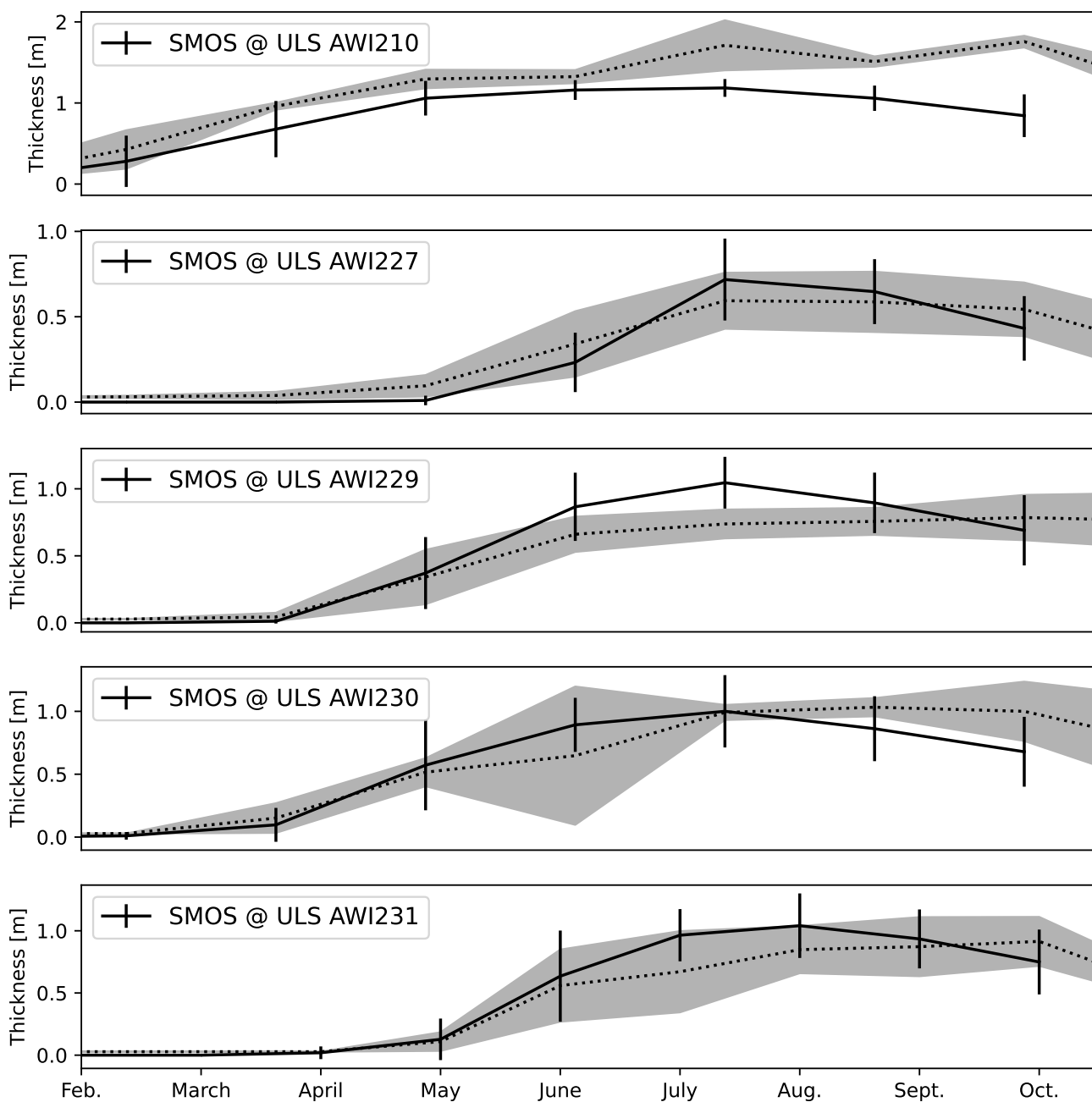
Figure 8. Climatological monthly mean ULS and SMOS sea-ice thickness version v3.3. The shading and the bars indicate the interannual variability (standard deviation) of ULS and SMOS sea-ice thickness respectively.
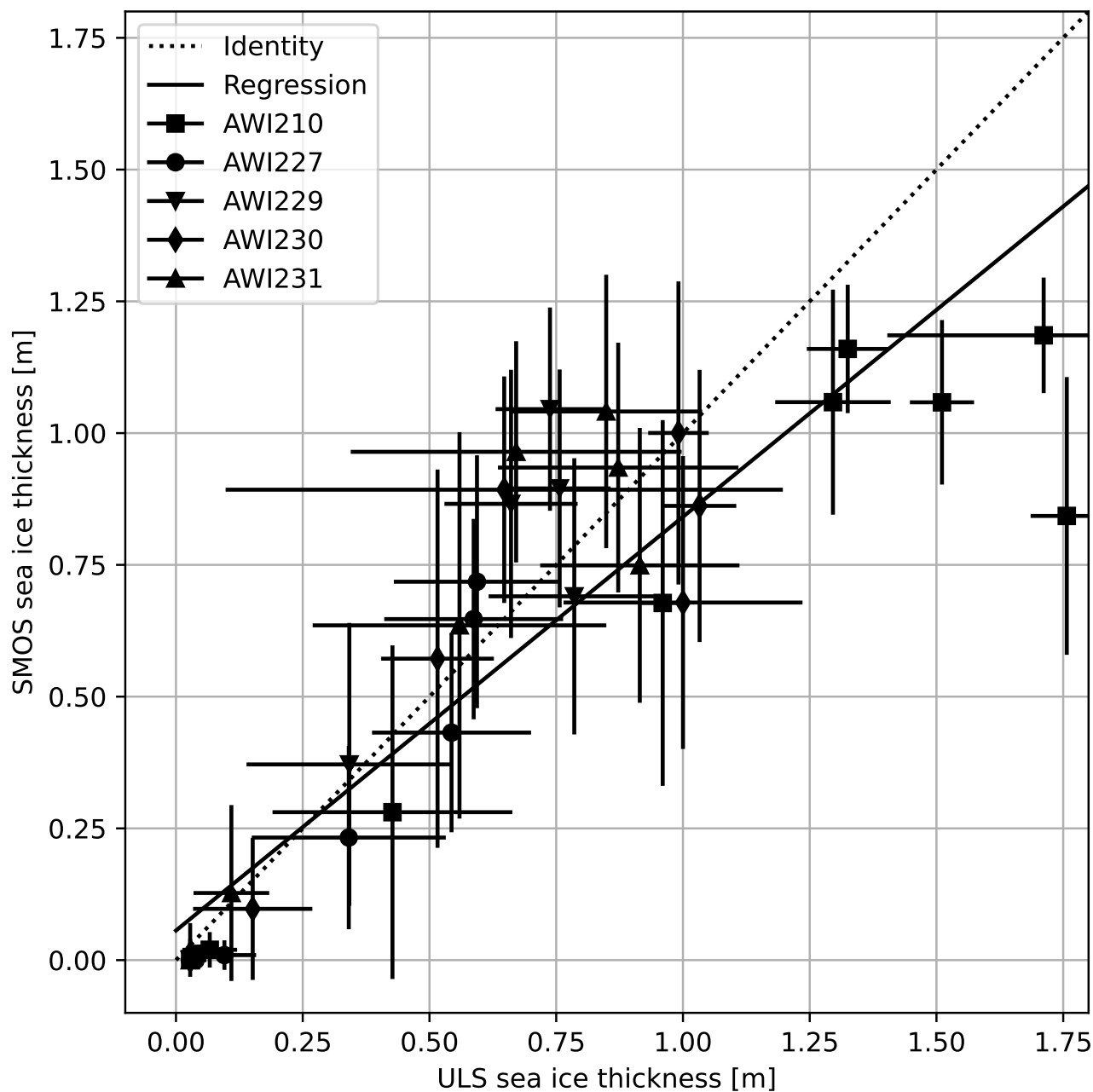
Figure 9. Scatterplot comparisons between climatological monthly mean ULS and SMOS sea-ice thickness. The bars indicate the interannual variability (standard deviation).
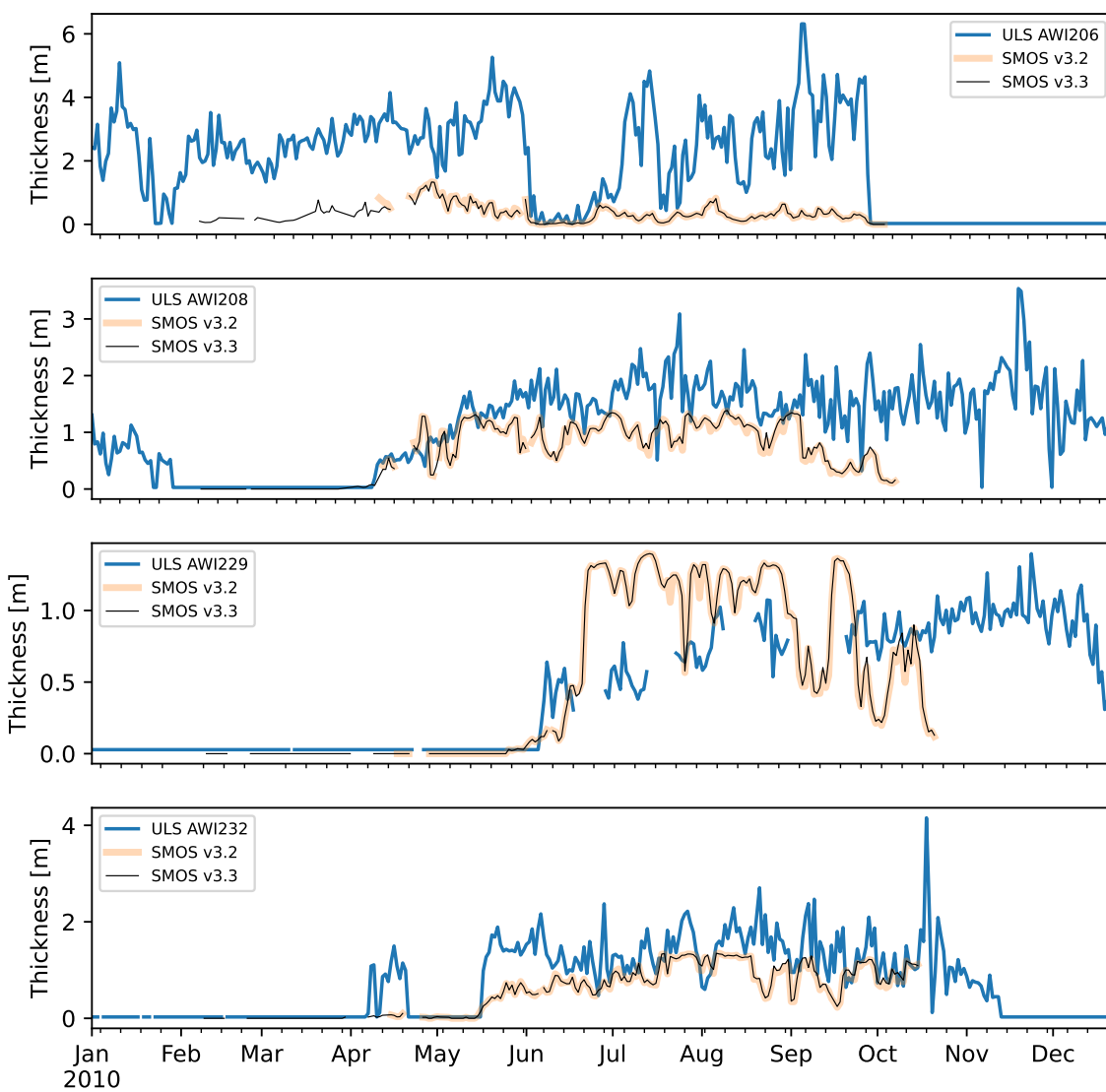
Figure 10. ULS and SMOS daily mean sea-ice thickness time series for the year 2010. Two different SMOS versions are shown.
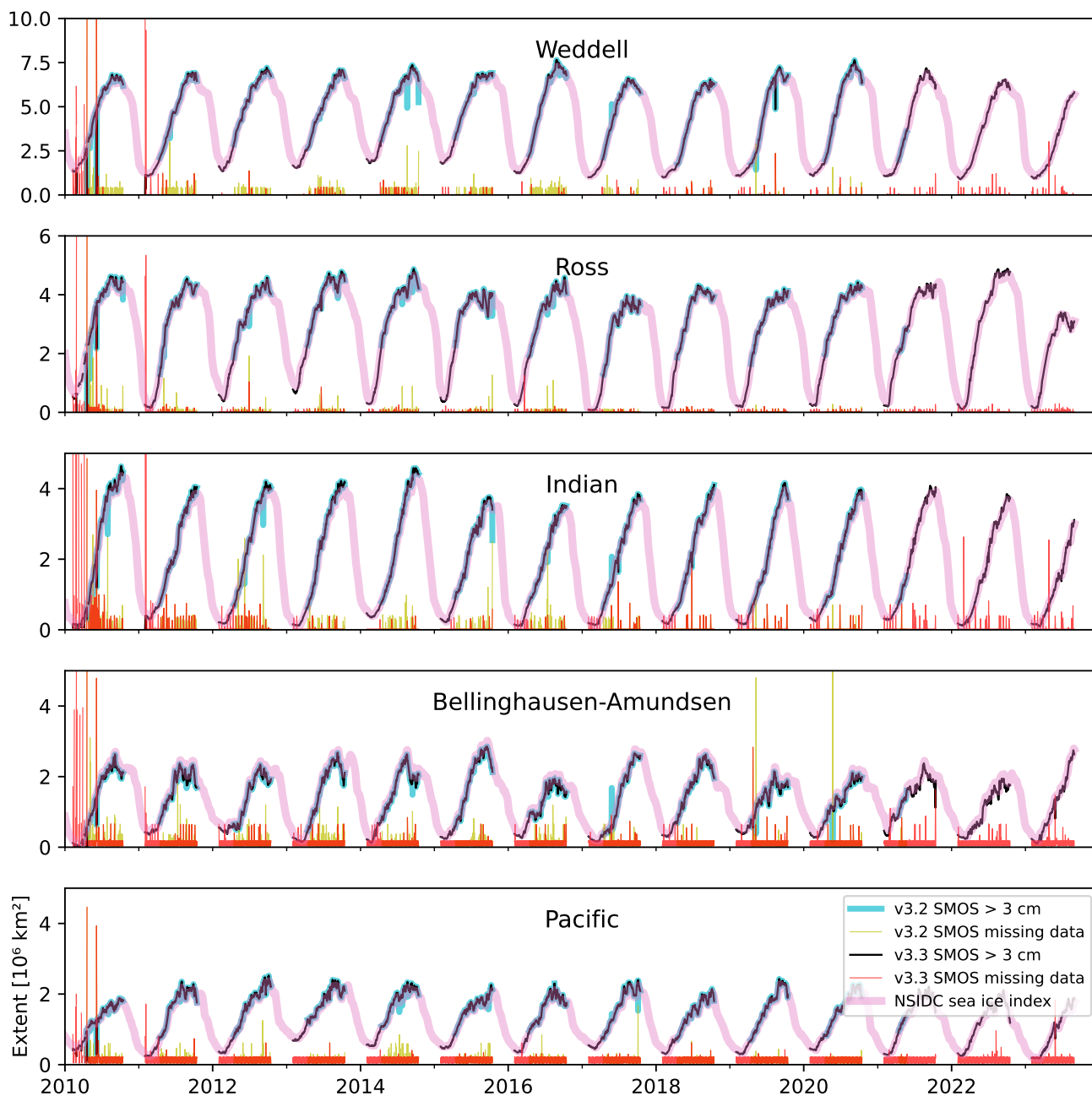
Figure 11. Regional sea-ice extent time series used for quality control. The regional NSIDC Sea Ice Index is shown in pink overlaid with the SMOS sea-ice extent in cyan and black for version v3.2 and v3.3, respectively. The yellow and red vertical lines indicate the number of missing data in terms of equivalent area for version v3.2 and v3.3, respectively.
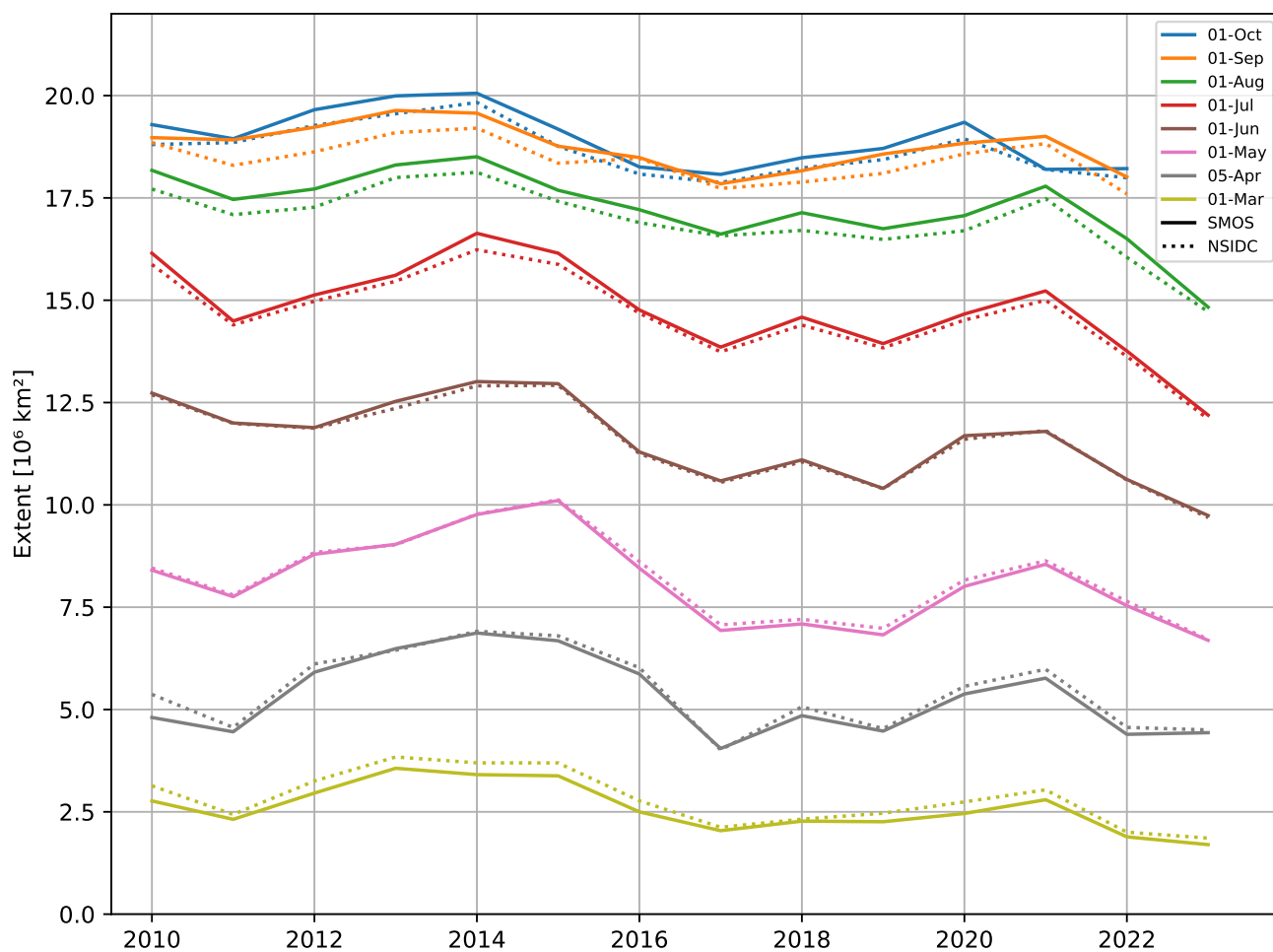
Figure 12. Total sea-ice extent time series used for quality control. The NSIDC Sea Ice Index (dash-dotted line) is shown with the SMOS sea-ice extent (solid line) color-coded for different dates, respectively. The extents for the first day of the month are shown. For April the 5th is selected due to missing data for the 1st-4th in 2010. Data for September and October 2023 are not yet available (August 2023).